Scientific Research Publishing

Advances in Remote Sensing, 2025, 14(3), 103-128
https://www.scirp.org/journal/ars
ISSN Online: 2169-2688
ISSN Print: 2169-267X

Assessment and Prediction of Effects of Geo-Environmental Hazards on Road Infrastructure Using an Ensemble Modeling Approach: A Case Study of Limuru - Mai Mahiu - Narok Road and Its Environs, Kenya

Evangeline Muthoni Njeru[1*], Daniel O. Olago[1], John P. O. Obiero[2], Lydia Olaka[3]

[1]Institute for Climate Change and Adaptation, University of Nairobi, Nairobi, Kenya
[2]Department of Environmental and Biosystems Engineering, University of Nairobi, Nairobi, Kenya
[3]Department of Geoscience and the Environment, Technical University of Kenya, Nairobi, Kenya
Email: *nj.evangeline@gmail.com

How to cite this paper: Njeru, E.M., Olago, D.O., Obiero, J.P.O. and Olaka, L. (2025) Assessment and Prediction of Effects of Geo-Environmental Hazards on Road Infrastructure Using an Ensemble Modeling Approach: A Case Study of Limuru - Mai Mahiu - Narok Road and Its Environs, Kenya. *Advances in Remote Sensing*, **14**, 103-128.
https://doi.org/10.4236/ars.2025.143007

Received: May 13, 2025
Accepted: August 3, 2025
Published: August 6, 2025

Abstract

In pursuit of a climate-resilient road infrastructure, the present study focused on the assessment and prediction of the aggregated effects of flooding and land subsidence on the Limuru - Mai Mahiu - Narok road in Kenya. The study used datasets which include: rainfall, land use land cover, normalized difference vegetation index, curve numbers, topographic wetness index, river density, slope, slope-length factor, soil texture, landforms, sediment transportation index and lineaments. A GIS-ensemble modeling approach coupling the multi-criteria decision analysis (MCDA) and principal component analysis (PCA) was used to simulate the combined effects of flooding and land subsidence on the road infrastructure for the year 1991, 2002, 2011 and 2021. Cellular automata-Markov chain analysis was used to predict the combined effects of flooding and land subsidence for the year 2030. The results revealed that the Limuru - Mai Mahiu - Narok road was prone to moderate, high and extremely high vulnerability levels. The vulnerability was dire in the year 2002 where about 77.4% of the road's manifested moderate, high and extremely high vulnerability levels. Besides, the road was least susceptible in the year 2021 since only about 49.1% of its length revealed moderate, high, and extremely high vulnerability levels. The prediction results depicted that by the year 2030, the length of the road infrastructure that would be vulnerable to moderate, high, and extremely high levels would increase by about 13.52%. The research findings provide essential information that would assist in the identification and

implementation of appropriate engineering and non-engineering interventions to the affected sections, thus promoting resilience of the road.

Keywords

Environmental Hazard, Road Infrastructure, Vulnerability, Prediction, Multi-Criteria Decision Analysis, Principal Component Analysis, Markov Chain Analysis

1. Introduction

Geo-environmental hazards are natural catastrophes occasioned by natural processes and anthropogenic activities happening in the hinterlands [1]. Geo-environmental hazards subject natural and built-up environments to detrimental effects which affect their resilience and qualities, thus jeopardizing the sustainability of the socio-economic development [2]. Upward trends of geo-environmental hazards pose threats to the lives and safety of people and properties [3]. Some of geo-environmental disasters which disrupt natural and man-made environments include flooding [4], land subsidence [5], pollution [6] among others.

Flooding overtops and deposits materials collected from hinterlands on the low-lying regions, and when unmanaged, exacerbates the health of both natural and built-up environments [7]. Frequent flooding poses risks on ecosystems and damage land cover, land uses, life, infrastructure, and reduces the anticipated lifespans of a built-up infrastructure [8]. Moreover, land subsidence is dictated by natural processes and anthropogenic activities which culminate in the movement of discrete segments of the ground surface [9]. Land subsidence mostly occurs in regions dominated by loose and pervious rocks [10], seismic waves [11], volcanic activities and land use activities such as drilling of boreholes, geothermal wells, quarries and mining activities [12]. Therefore, geo-environmental hazards pose significant threats to sustainable land use and management such as road infrastructure [13].

Roads are long-lived investment planned and constructed with anticipation that they would promote sustainable socio-economic development [14]-[16]. They are ecologically sensitive to geo-environmental hazards which affect their resilience, functionality and serviceability, despite efforts put to curb the occurrence of these disasters during planning, designing and construction stages [8]. For instance, flooding overtops and deposit materials on road's pavement which negatively affects the asphalt's durability and strength over time [17]. Moreover, the untimely occurrence of fissures on road's pavement is an indicator of the road failure [18]. Fissures are caused by sudden land subsidence attributed to accumulated strains on the tectonic plates, which comprise the earth's crust [19].

These hazards impair the stability and sustainability of road infrastructures, and pose risks to environment and traffic safety [18]. For instance, frequent flooding and land subsidence dilapidate roads' conditions, lower roads' safety, snarl-up

traffic flow, and increase operation and maintenance costs [20]. Therefore, the assessment of roads' vulnerability to natural disasters such as flooding and land subsidence should be prioritized and initiated at all stages of road's development [21]. This would prompt the identification of appropriate engineering and non-engineering interventions suitable for rehabilitating and alleviating road infrastructure from the effects of geo-environmental hazards [22] [23].

The review of global, regional and local studies exhibits that many roads' infrastructures are adversely damaged by untimely and uncontrolled flooding and land subsidence [14] [18] [19] [24]. [25] assessed the disruptive impacts of flooding on road infrastructure in Newcastle city council, United Kingdom using a flood depth-speed reduction function. The study deduced that floods induce delays to vehicle's speed escalated with an increase in flood depth. [26] monitored the flood exposure on road infrastructure in Switzerland using a network-based approach which identified road networks exposed to flooding and which required engineering and non-engineering interventions to reduce the risks. [27] researched on the environmental impact of flooding on transportation land use in Benin city, Nigeria through the administration of questionnaires based on the random sampling technique. The research findings reviewed that illegal disposal of refuse on drainage channels, high rainfall intensity, lack or ineffective drainage channels were the major causal of flooding on transportation network in the region. [19] monitored land subsidence rates along a road infrastructure in Xiding district in Tianjin, China. The research findings depicted a significantly uneven land subsidence pattern along the road infrastructure attributed to geological and land use activities such as ground water pumping in the region. The affected sections disrupted the mobility of goods and services and increased the maintenance cost. Moreover, [28] researched on effects of long rainy season to hydrological changes and land subsidence using global positioning systems (GPS) and interferometric synthetic aperture radar (InSAR) in Kenya. The research findings revealed a positive linear relationship between land subsidence and flooding which culminated to instability of the earth's surface during long rainy season.

Spectrum of researches have used GIS-multi-criteria decision analysis (MCDA) technique to simulate floods and land subsidence susceptibility maps [4]. The GIS-MCDA derives the significance level of each causal factor to the occurrence of flooding and land subsidence [29]. Despite, the fact that this method has been adopted by many studies, it falls short of being subjective, and thus its results may vary depending on the expert level of knowledge and experience [30]. Another method commonly used for determining the importance level of a contributing factor is the Principal Component Analysis (PCA). It is a multivariate tool used for reducing data dimensionality in a set of contributing factors. Its strength is based on the fact that it is objective and unaffected by measurement units of causal factors [28]. The only problem of PCA is the fact that it does not account for the domain knowledge.

From the review of past empirical studies, it's categorically clear that studies on

flooding and land subsidence had been done, but little has been done on assessing the aggregated effects of flooding and land subsidence on road infrastructure [19] [25]. Therefore, the present study focuses on the assessment and prediction of the aggregated effects of flooding and land subsidence on the Limuru - Mai Mahiu - Narok road using an ensemble modeling approach coupling the MCDA and PCA. The ensemble approach aimed at minimizing the subjectivity of MCDA model while addressing the issue of lack of domain knowledge in the PCA-based approach. The outcome of present study would aid in earmarking road's sections vulnerable to aggregated effects of geo-environmental hazards in order to aid in identifying the appropriate engineering and non-engineering interventions.

2. Data and Methodology

2.1. Description of the Study Area

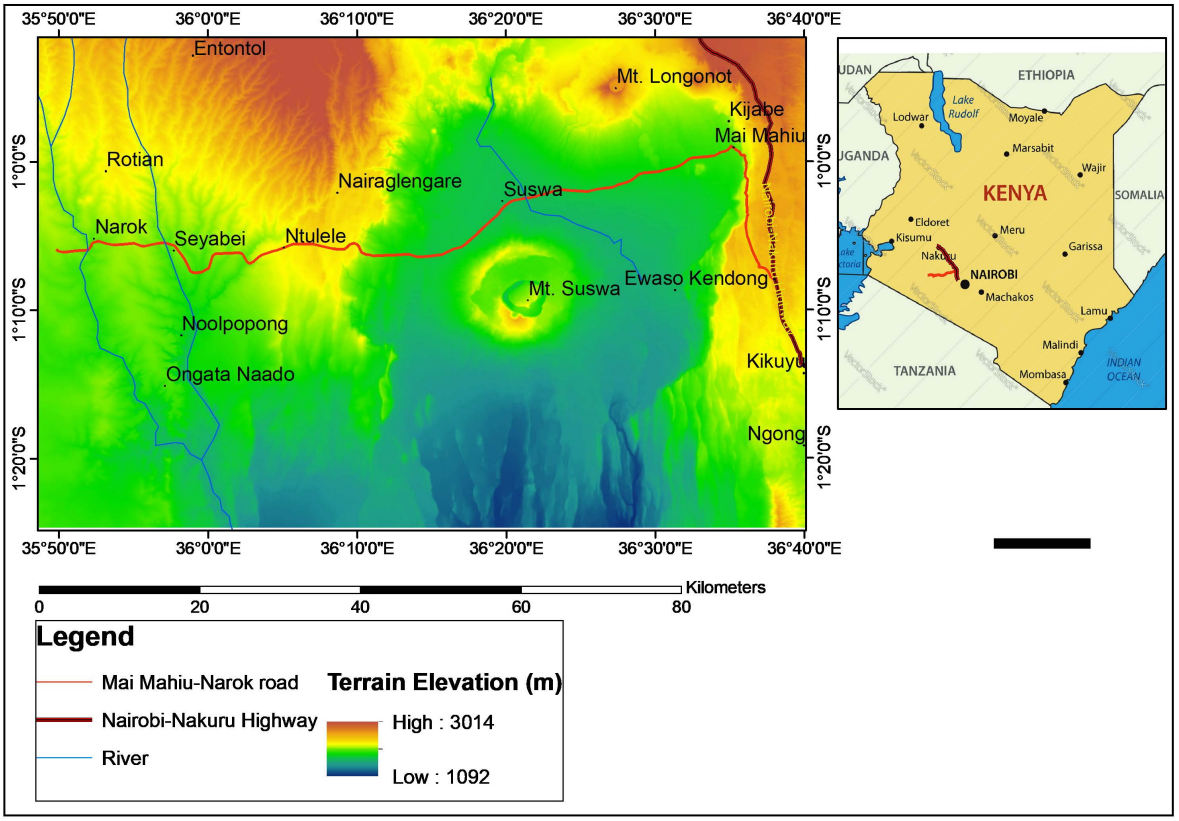

Figure 1. Location map for Limuru - Mai Mahiu - Narok road.

The focus of the present study is to assess and predict the aggregated effects of geo-environmental hazards, and in particular the flooding and land subsidence on the Limuru - Mai Mahiu - Narok road. This road is a bitumen standard infrastructure that is approximately 114 km long, which connects three Counties namely: Kiambu, Nakuru and Narok in Kenya [31]. The road is strategically located in a region defined by geographic coordinates (1˚00'00"S - 1˚10'00"S and 36˚0'00"E - 36˚45'00"E) (**Figure 1**). It branches from the Nairobi-Nakuru highway

at Kamadura, and traverse through a heterogeneous landscape comprising of escarpments, mountains, hills, gorges, and relatively flat plains [31]. The rainfall in the vicinity is bimodal with long and short rains received between March-May and October-November, respectively [31]. Besides its hinterlands are undulating with three distinct highest elevations points at Mt. Longonot (2716 m), Mt. Suswa (2357 m) and Olkaria hill (2454 m) [32].

The geological setting of the hinterlands is heterogeneous comprising products of volcanic activities such as caldera and mafic lavas, and deposited silt at low-lying regions [33]. Moreover, the hinterland is subjugated by loamy soil, ash and friable clay, with an exception of a fraction of the region which is dominated by porous and low water holding capacity soil.

2.2. Description of the Datasets

The template is used to format your paper and style the text. All margins, column widths, line spaces, and text fonts are prescribed; please do not alter them. You may note peculiarities. For example, the head margin in this template measures proportionately more than is customary. This measurement and others are deliberate, using specifications that anticipate your paper as one part of the entire journals, and not as an independent document. Please do not revise any of the current designations.

Table 1. Specifications of datasets used for assessing the vulnerability of Limuru - Mai Mahiu - Narok road to the aggregated effects of flooding and land subsidence.

ID	Data	Specification	Sources
1.	Multispectral Landsat data (1991-2021)	Geo tiff, WGS 1984, GCS coordinate system, (March-May), Scenes 168061, 169060,169061	U.S Geological Surveying
2.	Station rainfall data (1991-2021)	Tabular data with GPS coordinate	Kenya Meteorological department
3.	Gridded rainfall data (1991-2021)	Gridded, WGS 1984 UTM zone 37N from the year 1990-2021	CHIRPS blended satellite-station precipitation
4.	30m Digital elevation model	Shuttle Radar Transmission mission gridded DEM, WGS 1984, GCS coordinate system	ALASKA facility services
5.	Geological map	Scanned, WGS 1984, GCS coordinate system (map scale 1:500,000)	The Geological Society of America Digital Maps (Alexandria Guth, Dept. of Geology, Michigan Technological University). doi.10.1130/2014.DMCH016
6.	Soil data	Shapefile, WGS 1984, GCS coordinate system (maps scale 1:500,000)	Food and Agriculture Organization (FAO)
7.	River networks	Shapefile, Arc 1960 UTM zone 37N	Kenya GIS data
8.	Road network	Shapefile, Arc 1960 UTM zone 37N	Kenya GIS data
9.	Collected Floods and fissures GPS locations	Point data; Arc 1960 UTM zone 37N	Field survey
10.	Quantitively data	Structured questionnaire	Fieldwork

The present study used various contributing factors to assess and predict the susceptibility of Limuru - Mai Mahiu - Narok road to the effects of geo-environmental hazards composing of flooding and land subsidence. Datasets which include surface runoff, land use land cover (LULC), normalized difference vegetation index (NDVI), slope, topographic factor (LS), curve numbers, soil(texture), landforms, river density, topographic wetness index (TWI) and sediment transportation index and lineament density were used (**Table 1**). Slope, lineaments, LS and TWI were extracted from 30 m digital elevation model sourced from Alaska facilities services, https://asf.alaska.edu/; LULC and NDVI were extracted: from multispectral Landsat imageries sourced from the United State Geological Survey, https://glovis.usgs.gov/; soil texture and landforms were extracted from the documented attributes of soil data obtained from Food Agriculture Organization (FAO); station-based rainfall data from the Kenya meteorological department; gridded rainfall data sourced from the Climate Hazards Group Infrared Precipitation with station data (CHIRPS, https://www.chc.ucsb.edu/data/chirps/; surface runoff simulated using the Soil Conservation Services-Curve number model; river and roads data sourced from Kenya open GIS data, https://data.humdata.org/dataset/kenya, and geo-environmental hazards presence and absence data collected using GPS during field survey.

2.3. Methodology

2.3.1. Data Pre-Processing and Harmonization

Before carrying out data analysis, multispectral Landsat imageries were corrected for radiometric distortions commissioned by the characteristics of imaging conditions and systems. A Fast Line-of-sight Atmospheric Analysis of Hypercubes (FLAASH) model was used to correct the radiometric and atmospheric noise such as cloud cover, scanlines, and atmospheric haze in the spectral bands. Besides, in order to facilitate data overlay, the acquired satellite imageries were geo-referenced and projected to a common coordinate system, that is Universal Transverse Mercator (UTM) coordinate system, zone 37N using the Arc 1960 reference ellipsoid as the datum. Additionally, the raster datasets were resampled using bi-linear interpolation approach to a spatial resolution of 30 m. Lastly, the soil and geological shapefiles were rasterized using the appropriate attribute in order to facilitate further data analysis.

2.3.2. Data Analysis

1) Extraction of land use land cover and vegetation indices

The present study adopted maximum likelihood classification algorithm which is a type of supervised classifications tools to generate land use land cover (LULC) from the composite images for 1991, 2002, 2011 and 2021. Prior, to the application of the algorithm, 70% of the collected GPS location data during field survey and from google maps were used as training dataset for the supervised classification and six categories were generated namely bare land, forest, built-up area, agriculture, grassland and water. The remaining 30% ground truthing data was used to

validate the classified LULC, whereby Kappa coefficients, overall accuracy, producer accuracy and the user accuracy were used to ascertain the degree of reliability of the classification process.

Moreover, the normalized difference vegetation indices (NDVI) were extracted using Equation (1). NDVI was calculated using the red band near infrared band and values ranges between −1 to +1, where −1 to 0 denotes no vegetation, 0 - 2 denotes soil, 2 - 3 represents a mixture of soil and vegetation, 3 - 5 signifies moderately vegetated areas, and the range between 0.5 - 1 denoted health and highly vegetated regions

$$\mathrm{NDVI} = \left(\mathrm{NIR} - \mathrm{RED}\right)/\left(\mathrm{NIR} + \mathrm{RED}\right) \tag{1}$$

where NIR denotes near infrared band and RED denotes red band of the multispectral imageries.

2) Extraction of topographic attributes from DEM

The physiographic features such as slope, topographic wetness index (TWI) and slope-length factor (LS) were extracted from the Digital Elevation Model (DEM). The slopes of hinterlands were extracted in degrees and in percentage for use in the subsequent analysis, while the topographic factor (LS) was extracted using Equation (2).

$$\mathrm{LS} = 1.4 \times \left(\alpha\beta\phi/22.1\right)^{0.4} \times \left(0.01745 \sin\left(\mathrm{slope}\left(\theta\right)\right)/0.09\right)^{1.4} \tag{2}$$

where α is the flow accumulation, β denotes the spatial resolution (30 m) of DEM, and ϕ denotes the slope in percentage, respectively.

Moreover, the topographic wetness index (TWI) was extracted using Equation (3) [4], where $\propto$ denotes the cumulative upslope draining area per contour length (unity), and β denotes the slope angle

$$\mathrm{TWI} = \ln\left(\propto/\tan\beta\right) \tag{9}$$

High TWI values reveal high susceptibility to water accumulation and stagnation depicting poor drainage and water-logged hinterlands which possess high probability of flooding while low values denote regions less susceptible to water flooding.

3) Extraction of hydrological response units (HRUs) and curve numbers (CN)

HRUs values were derived from a combination of land use land cover (LULC), hydrological soil groups (HSGs) and slope [34]. Soil texture was classified into hydrological soil groups A, B, C, and D based on the hydraulic conductivity [35]. Different land use and land cover respond differently to surface runoff, infiltration and interception. The extracted LULC raster layer was vectorized into polygons and combined with HSGs using the geometric intersection. The output was new polygons comprising of attributes of HSGs and LULC which were subsequently used to generate HRUs [35]. Using the field calculator in ArcGIS software, HRUs were assigned CN values as dictated in the Soil Conservation Services (SCS) look-up table [36]. [37] method was used to correct for slope effects using Equation (4).

$$\mathrm{CN}_{\mathrm{Slope}} = \mathrm{CN}\left(322.79 + 15.63\alpha\right)/\left(\alpha + 323.52\right) \tag{4}$$

where CN signifies curve number and α (m·m^{-1}) denotes slope.

4) Estimation of surface runoff using the ArcCN-runoff tool

The ArcCN-runoff tool was used to estimate the potential water retention (S) using Equation (5) [36].

$$S_{0.20} = \left(25400/\mathrm{CN}_{\mathrm{Slope}}\right) - 254 \tag{5}$$

Equation (5) estimated the potential maximum retention (S0.20) based on assumption of 20% which was proved to be overestimating. Using Equation (6), the $S_{0.20}$ was converted to the potential maximum retention ($S_{0.05}$) based on 5% water retention, which was proved to yield better results compared to the former [38]. The conversion was attributed to the fact that the look up table for CN values was based on $S_{0.20}$. The potential surface runoff was then simulated using Equation (7) using the CN-runoff tool which is a spatial extension tool for ArcMap version 10.4.

$$S_{0.05} = 1.33 S_{0.20}^{1.15} \tag{6}$$

$$Q = \left(P - 0.05 S_{0.05}\right)^2 \Big/ \left(P + 0.95 S_{0.05}\right) \tag{7}$$

where: P is rainfall (mm) and Q is potential surface runoff.

5) Extraction of lineament density

Lineaments which define fissures or fractures on the geological settings were extracted using two approaches [39]. The first approach involved manual digitization of lineaments from scanned existing geological map of the study area in a GIS environment. The second approach involved the automatic extraction of lineaments from the DEM using Geomatica line tool that is compatible with the ArcGIS software [40]. The hill shade relief analysis was carried out using solar elevation angle (angle to the horizon) and solar illumination angle that is, the orientation of the sun's rays to the north. To enhance the lineaments in the derived hill shade, four sets of sun's azimuths that is, 0˚, 45˚, 90˚, 135˚ were used and the sun altitude was maintained at 45˚ [41]. Then using the Geomatica line tool which is an extension of spatial analyst tools in ArcGIS automatically extracted lineaments from hill shades setting a minimum length of 0.1km. Lastly, using the line density tool in ArcGIS, the lineament density raster layer was derived which was subsequently used in identifying regions vulnerable to land subsidence [40].

6) Extraction of river density from the existing rivers network

Using the line density geoprocessing tool in ArcGIS, river density was generated from the existing rivers networks that calculated the magnitude-per-unit area from the polyline features. The river density values range from 0 to a value representing the highest magnitude-per unit area from the river density.

7) Rasterization of soil texture and landforms

Soil data was rasterized into four main categories based on soil texture namely, clayey, loamy, silt and sand. Besides, using the attribute of landforms, the hinterlands were categorized in six categories namely, undulating, steep, rolling, flat, gently undulating and moderately undulating.

8) Extraction of sediment transportation index

Sediment transportation index (STI) was extracted using Equation (8) [22]. STI

manifests how deposition is triggered by slope and landscape configuration of the hinterlands.

$$\mathrm{STI} = \left(A_S/22.1\right)^{0.6} \times \left(\sin\beta/0.0896\right)^{1.3} \quad (8)$$

where A_S denotes the upstream area and β represents the slope angle at a certain pixel.

9) Preference judgement and reclassification of the causal factors

The scores used for reclassifying the causal factors to the occurrence of flooding and land subsidence were assigned using a nine-weighted scale as illustrated in Table 2 [42].

Table 2. Saaty scale for ranking the preference of contributing factors to the occurrence of geo-environmental hazards.

Scale	Meaning	Related flood's vulnerability level
1	Equally important	Extremely low
3	Moderately important	Low
5	Important	Moderate
7	Very Strongly important	High
9	Extremely important	Extremely high
2, 4, 6, 8	Intermediate values between adjacent scales	

Besides, the causal factors were reclassified by assigning values which were in tandem with probability of pixel contributing to the occurrence of flooding and land subsidence (Table 3).

Table 3. Contribution of causal factors to the occurrence of flooding and land subsidence in the hinterlands.

Factors		Criteria scales and scores in parentheses ()					Source
Slope	(˚)	0 - 3 (9)	3 - 8 (7)	8 - 15 (5)	15 - 25 (3)	25 - 87 (1)	[43]
Surface Runoff	mm	<207.11 (1)	207.51 - 399.73 (3)	399.73-569.07 (5)	569.07 - 894.01 (7)	>894.01	Natural breaks [8]
LULC	level	Forests (2) Grasslands (3)	Shrubs (4)	Agriculture (5)	Bareland (7) Built up areas (8)	Water (9)	[43]
Curve number	level	<40.37 (1)	40.37 - 55.28 (3)	55.28 - 70.19 (5)	70.19 - 85.09 (7)	85.09 - 100 (9)	Natural breaks [8]
Topographic factor	level	<11.41 (9)	11.41 - 31.40 (7)	31.40 - 111.32 (5)	111.32 - 285.43 (3)	>285.43	Natural breaks [8]
Topographic wetness index	level	<2.8 (1)	2.8 - 4.2 (3)	4.2 - 6.0 (5)	6.0 - 8.2 (7)	>8.2 (9)	[43]
River Density	Km/km^2	0 - 0.70 (1)	0.7 - 1.0 (2)	1 - 1.25 (3)	1.25 - 1.52 (4)	>1.52	[4]
NDVI	level	<−0.02 (9)	−0.02 - 0.30 (7)	0.3 - 0.4 (5)	0.40 - 0.5 (3)	>0.5 (1)	[4]
Landform	level	Ridges and high-gradient hill/mountain (1)	Mountainous highlands (3)	Low-gradient mountains (5)	Plateau (7)	Plains (9)	[4]
Soil Texture	level	Sandy (1)	Loamy (3)	Clayey (5)	Very Clayey (7)		[43]
Sediment transportation index	level	<528.80 (1)	528.80 - 5816.76 (3)	5816.76 - 17450.27 (5)	17450.27 - 34900.54 (7)	>34900.54 (9)	Natural breaks [8]
Lineaments density	level	0 - 0.16 (1)	0.16 - 0.46 (3)	0.46 - 0.77 (5)	0.77 - 1.16 (7)	1.16 - 2.32 (9)	Natural breaks [8]

2.3.3. Modeling the Vulnerability of Road Infrastructure to Flooding and Land Subsidence Using Analytical Hierarchical Process

The study used the analytical hierarchical process (AHP) to assess the vulnerability of the Limuru - Mai Mahiu - Narok road to flooding and land subsidence [4]. For flooding mapping, eleven contributing factors which include: surface runoff, slope, LULC, slope-length factor (LS), river density, curve numbers, topographic wetness index, landforms, sediment transportation index and soil texture were used. To map the vulnerability of the Limuru - Mai Mahiu - Narok road and its environs to land subsidence nine causal factors which include: surface runoff, lineament density, lithology, land use land cover, length-slope factor, curve numbers, topographic wetness index, stream density and soil types were used. Then pairwise comparison tables based on experts' judgement obtained from a spectrum of professionals in environmental engineering (2), transportation engineering (7), geological science (1), geomatics engineering and geoinformatics science (3), and structural engineering (2) were derived to determine the level of significance of each contributing factor to flooding and land subsidence. Prior to this, the causal factors for flooding as well as for land subsidence were reclassified and standardized using the nine-point weighted scale (1 to 9) to facilitate their comparison as shown **Table 4** and **Table 5** [44]. Additionally, the consistency ratios (C.R) were computed to assess the degree of acceptability (C.R ≤ 0.1) of results using Equations (9) and (10) [29].

$$\text{C.I} = \left(\lambda_{\max} - n\right)/\left(n-1\right) \tag{9}$$

$$\text{C.R} = \text{C.I}/\text{R.I} \tag{10}$$

where $\lambda_{\max}$ is the largest eigen value, n is the number of items being compared in the matrix, R.I is the random consistency index.

Table 4. Derived eigenvectors in the pairwise comparison matrix for assessing the vulnerability of road infrastructure to flooding.

	SL	SR	LULC	CN	LS	TWI	RD	NDVI	LF	ST	STI	SUM	CW
SL	0.14	0.25	0.08	0.08	0.10	0.13	0.12	0.14	0.16	0.12	0.11	1.44	0.13
SR	0.07	0.13	0.25	0.08	0.10	0.13	0.12	0.14	0.16	0.17	0.11	1.45	0.13
LULC	0.14	0.04	0.08	0.31	0.20	0.07	0.04	0.05	0.05	0.12	0.08	1.19	0.11
CN	0.14	0.13	0.02	0.08	0.20	0.13	0.12	0.14	0.05	0.04	0.08	1.14	0.10
LS	0.14	0.13	0.02	0.04	0.10	0.13	0.12	0.14	0.16	0.12	0.08	1.18	0.11
TWI	0.07	0.06	0.08	0.04	0.05	0.07	0.12	0.14	0.05	0.04	0.11	0.84	0.08
RD	0.05	0.04	0.08	0.03	0.03	0.02	0.04	0.02	0.05	0.17	0.03	0.55	0.05
NDVI	0.05	0.04	0.08	0.03	0.03	0.02	0.12	0.05	0.05	0.04	0.14	0.65	0.06
LF	0.14	0.13	0.25	0.23	0.10	0.20	0.12	0.14	0.16	0.12	0.11	1.70	0.15
ST	0.05	0.03	0.03	0.08	0.03	0.07	0.01	0.05	0.05	0.04	0.14	0.57	0.05
STI	0.03	0.03	0.03	0.03	0.03	0.02	0.04	0.01	0.04	0.01	0.03	0.30	0.03
SUM	1.00	1	1	1	1	1	1	1	1	1	1	11	1

Table 5. Derived eigenvectors in the pairwise comparison matrix for assessing the vulnerability of road infrastructure to land subsidence.

	SR	LNT	LIT	LULC	LS	CN	TWI	SD	ST	SUM	Relative weights	Weight (%)
SR	0.167	0.275	0.103	0.292	0.200	0.062	0.162	0.207	0.091	1.559	0.173	17
LNT	0.167	0.275	0.517	0.292	0.333	0.308	0.270	0.207	0.182	2.551	0.283	28
LIT	0.167	0.055	0.103	0.195	0.200	0.123	0.162	0.138	0.091	1.234	0.137	14
LULC	0.028	0.046	0.026	0.049	0.067	0.123	0.054	0.103	0.091	0.586	0.065	7
LS	0.056	0.055	0.034	0.049	0.067	0.185	0.162	0.103	0.091	0.802	0.089	9
CN	0.167	0.055	0.052	0.010	0.022	0.062	0.054	0.138	0.091	0.650	0.072	7
TWI	0.056	0.055	0.034	0.049	0.022	0.062	0.054	0.034	0.182	0.548	0.061	6
SD	0.028	0.046	0.026	0.016	0.022	0.015	0.054	0.034	0.091	0.333	0.037	4
ST	0.167	0.138	0.103	0.049	0.067	0.062	0.027	0.034	0.091	0.737	0.082	8
SUM	1	1	1	1	1	1	1	1	1	9	1	100

Where SL represents slope, SR is surface runoff, LULC is the and use land cover, CN is the curve number, LS is the topographic factor, TWI is the topographic wetness index, RD is river density, NDVI is the normalized difference vegetation index, LF is the landforms, ST is soil texture, STI is the sediment transportation index, LNT is the lineaments density and CW is the criteria weight.

The random factor of 1.51 was adopted to compute the C.I for floods mapping since coincided with the value set for eleven contributing factors (n), while a random index of 1.45 was adopted for land subsidence mapping since was derived using nine causal factors [42]. Using the derived weights in Table 4 and Table 5, the floods and land subsidence vulnerability maps for 1991, 2002, 2011 and 2021 were simulated. The simulated floods and land subsidence vulnerability maps were then reclassified into five levels of vulnerability (extremely low, low, moderate, high and extremely high) using the [45] scaling approach.

2.3.4. Modeling the Vulnerability of Road Infrastructure to Flooding and Land Subsidence Using Principal Component Analysis

Using the eleven and nine factors similar to those used in AHP process, the principal component analysis (PCA) was performed to model the floods and land subsidence vulnerability maps, respectively, for 1991, 2002, 2011 and 2021. The manipulation was carried out using the PCA tool in ArcGIS software. The PCA-based floods vulnerability maps manipulated the eleven contributing factors (Table 6) which end products were 11 × 11 matrix of factors eigenvectors and 11 × 1 matrix of percentages of eigenvalues for the principal component (PC) layers [46]. Moreover, the PCA-based land subsidence maps used nine contributing factors (Table 7) whose results were 9 × 9 matrix of factors eigenvectors and 9 × 1 matrix of percentages of eigenvalues for the principal component (PC) layers.

To minimize the uncertainties in the level of influence of driving factors due to their spatial-temporal variations over epochs under investigation, geometric mean

was executed to the derived criteria weights for each contributing factor based on the outcome of four epochs considered as depicted by column 6 of Table 6 and Table 7 [22]. The derived geometric mean weights for contributing factors were normalized so that their sum yields 100% as depicted by column 7 of Table 6 and Table 7. Using the normalized criteria weights, the floods and land subsidence vulnerability maps were generated, respectively for 1991, 2002, 2011 and 2021. [42] reclassification criteria were applied to reclassify floods and land subsidence vulnerability levels such as the extremely low, low, moderate, high and extremely high.

Table 6. PCA-based criteria weights (%) for modeling flooding vulnerability mapping.

Contributing Factors	1991	2002	2011	2021	Criteria weights %)	Normalized weights (%)
Slope	16.18	17.05	13.61	13.73	15.07	15.25
Surface Runoff	16.57	10.88	18.40	17.36	15.49	15.68
LULC	8.07	8.22	12.42	10.52	9.65	9.77
Curve No.	13.46	16.85	13.56	13.69	14.32	14.50
LS Topography	0.90	0.95	0.76	0.76	0.84	0.85
TWI	12.54	13.21	10.55	10.64	11.68	11.82
River Density	1.41	1.49	1.19	1.20	1.32	1.33
NDVI	1.78	1.28	4.71	4.53	2.64	2.67
Landforms	17.54	17.90	15.10	17.76	17.03	17.24
Soil texture	11.54	12.16	9.71	9.80	10.75	10.88
Sediment	0.01	0.01	0.01	0.01	0.01	0.01
Total	100.00	100.00	100.00	100.00	98.79	100.00

Table 7. PCA-based criteria weights (%) modeling land subsidence vulnerability mapping.

Contributing factors	1991	2002	2011	2021	Criteria weights (%)	Normalized weights (%)
Surface runoff	14.13	15.83	13.58	15.93	14.83	14.97
Lineaments	16.42	18.67	16.82	16.92	17.18	17.34
Lithology	15.54	12.63	14.58	13.25	13.95	14.08
LULC	6.88	8.18	11.20	9.66	8.83	8.91
Slope	13.80	7.24	12.27	12.60	11.15	11.25
HRUs	11.48	10.70	12.23	12.56	11.72	11.83
TWI	10.70	13.15	9.51	9.76	10.69	10.79
Stream density	1.21	1.48	1.07	0.33	0.89	0.90
Soil Type	9.85	12.11	8.75	8.99	9.84	9.93
Total	100.00	100.00	100.00	100.00	99.10	100.00

2.3.5. Modeling the Combined Effects of Flooding and Land Subsidence on Road Infrastructure

This was achieved by aggregating both flooding and land subsidence vulnerability maps using a geometric mean approach illustrated in Equation (11).

$$agg_i = \left(fldv_i \times lsv_i \right)^{1/2} \tag{11}$$

where agg_i denotes the aggregated effects of flooding and land subsidence at a given epoch i, $fldv_i$ denotes the floods vulnerability maps at a given epoch and lsv_i denotes the land subsidence vulnerability map at a given epoch.

The aggregated vulnerability maps were validated using the collected flooding and land subsidence GPS locations. A contingency table composing of flood-zones, fault lines and fissures-zones, non-flood zones and non-fault lines and fissures prone zones was prepared. The validation was ascertained using Kappa statistics, overall accuracy, producer accuracy and user-accuracy. Besides, the combined floods and land subsidence vulnerability maps were reclassified using [42] approach into five classes namely, extremely low, low, moderate, high and extremely high levels. Lastly, the length (km) of the Limuru - Mai Mahiu - Narok road susceptible to each category of vulnerability was determined to aid in identifying sections that require immediate engineering and non-engineering interventions.

2.3.6. Prediction of the Combined Effects of Flooding and Land Subsidence on Road Infrastructure

First, the process involved the determination of the transfer matrix which expresses the change in state from one time (t1) to another time (t2) [47]. The Markov chain analysis was used to generate the transfer matrix which depends on the characterization of current and previous states as well as the neighborhoods. That is, Markov chain analysis generated the Markovian transition estimators which include: probability area matrix, transition suitability image, the Markov transition area files. These Markovian transition estimators were based on the aggregated effects of flooding and land subsidence vulnerability maps for 1991 and 2011 as the base images [48]. The present study used 20 years interval where the floods and land subsidence vulnerability maps for the year 1991 and 2011 were input in the Markov chain analysis tool to derive the transition suitability image and the Markov transition files as a transfer matrix.

The produced transition suitability image for 1991-2011, the Markov transition area files, and the combined floods and land subsidence vulnerability map for 2011 were input to the cellular automata (CA) tool to predict the aggregated floods and land subsidence vulnerability map for 2021. This was realized by setting the number of iterations as 10 denoting the time period between the year 2011 and 2021. Besides, a standard 5 × 5 contiguity cellular automata filter was employed to determine the weighted factor of transition which was computed based on the distance between the nuclear and adjacent cells [48]. The predicted maps for 2021 and the geometric mean based simulated maps for the same year were compared

to ascertain the degree of reliability of the prediction model. The validation was ascertained by computing Kappa coefficients values which include: Kno, Klocation, KlocationStrata, Kstandard and the average index.

Moreover, the future scenario for the aggregated floods and land subsidence vulnerability map for the year 2030, was generated using the base image of the aggregated floods and land subsidence vulnerability map for the year 2021, the produced transition suitability image and Markov transition areas files using CA-Markov chain analysis and setting the number of iterations as 9. The generated vulnerability map for the year 2030 was reclassified into five classes namely extremely low, low, moderate, high, and extremely high vulnerability levels. Lastly, the length of the Limuru - Mai Mahiu - Narok road that fell under each category of vulnerability was computed.

2.4. Results

2.4.1. Road's Vulnerability to the Combined Effects of Flooding and Land Subsidence

The results for the combined effects of flooding and land subsidence are shown in Figure 2. The values for the combined geo-environmental hazard maps ranged between 2 - 7.4 signifying extremely low and extremely high vulnerability levels, respectively (Figure 2(a)). Besides, the validation results between the collected GPS points and aggregated floods and land subsidence vulnerability map for 2021 are shown in Table 8. The validation results produced an overall accuracy of 86% and a Kappa coefficient value of 0.80 which were satisfactorily good. Additionally, the validation results generated producers' accuracies of 86.8%, 73.3%, 84.9% and 90.3% for flooded prone, non-flooded prone, land subsidence prone and non-land subsidence prone zones, respectively. Besides, the validation results produced users' accuracies of 80.0%, 73.3%, 90.1% and 90.9% for flooded prone, non-flooded prone, land subsidence prone and non-land subsidence prone zones, respectively.

Table 8. Contingency table composed between the collected flooding and land subsidence GPS reference data and aggregated floods and land subsidence vulnerability map for the year 2021.

Category	Flood prone zones	Non-flood prone zones	Subsidence prone zones	Non-subsidence prone zones	Sum
Flood prone zones	132	18	6	9	165
Non-flood prone zones	8	85	11	12	116
Subsidence prone zones	3	7	163	8	181
Non-subsidence prone zones	9	6	12	271	298
Sum	152	116	192	300	**760**

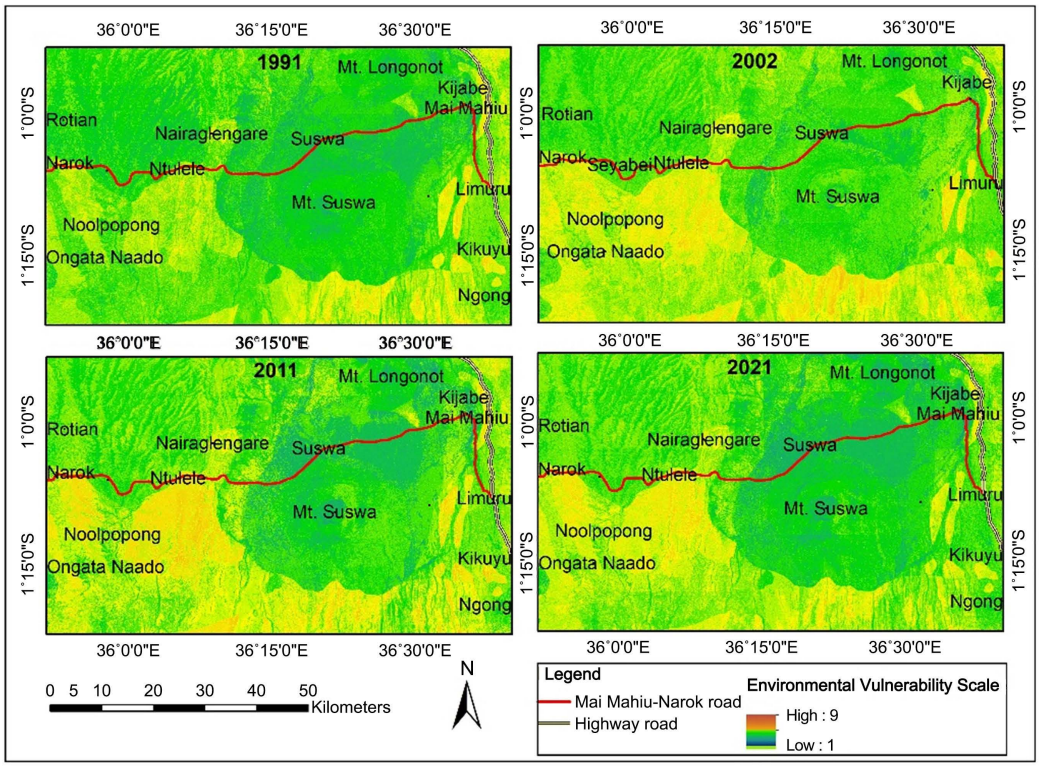

(a)

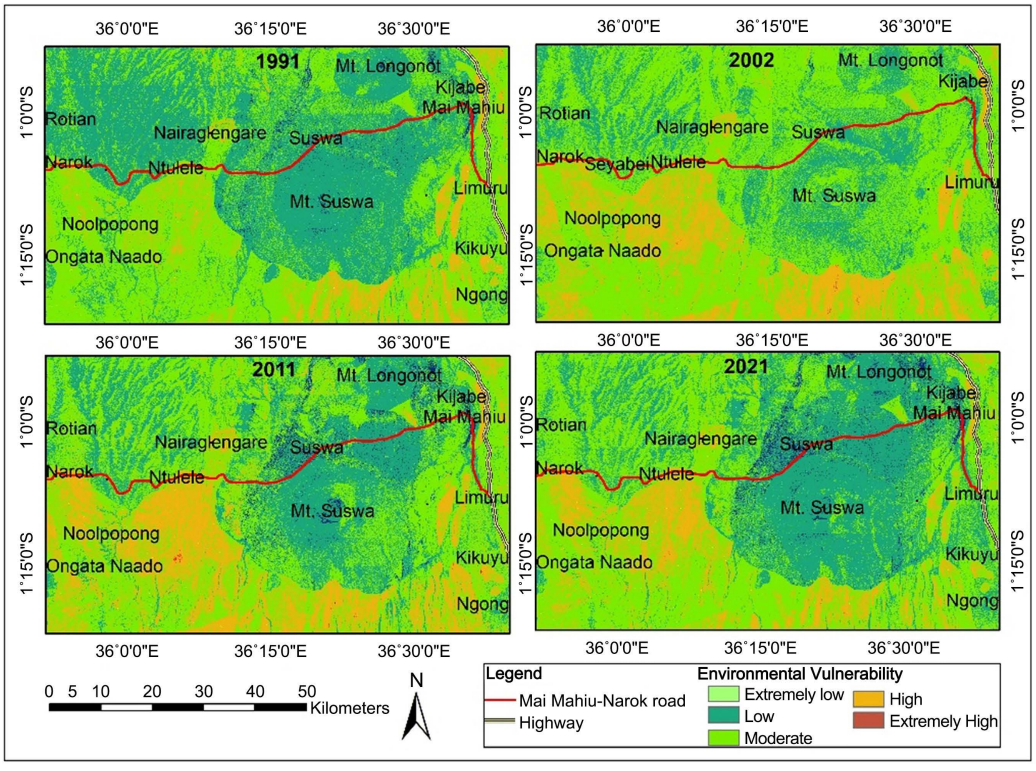

(b)

Figure 2. (a) Combined effects of floods and land subsidence geo-environmental hazards on Limuru - Mai Mahiu - Narok road and its environs, (b) Reclassified aggregated geo-environmental vulnerability maps for Limuru - Mai Mahiu - Narok Road and its environs.

The reclassified results revealed that areas of about 0.09% - 1.89%, 20.66% - 40.49%, 50.53% - 62.79%, 7.97% - 19.75%, and 0.00% - 0.03% of the hinterlands experienced extremely low, low, moderate, high, and extremely high vulnerability levels, respectively (Figure 3). Besides, the results manifest that the most vulnerable regions to the combined effects of flooding and land subsidence include: Kijabe, Mai Mahiu, Kikuyu, Ngong, Ewaso Kendong, Nairaglengare, Ntulele, Ongata Naado, Noolpopong and Narok (Figure 2(b)). The year 1991 and 2021 registered more than half of hinterlands exhibiting extremely low and low vulnerability levels to the combined effects of flooding and land subsidence. Besides, the year 2002 and 2011 manifested a substantial size of hinterlands of about 16.47% and 19.8%, respectively depicting high and extremely high vulnerability levels to geo-environmental hazards.

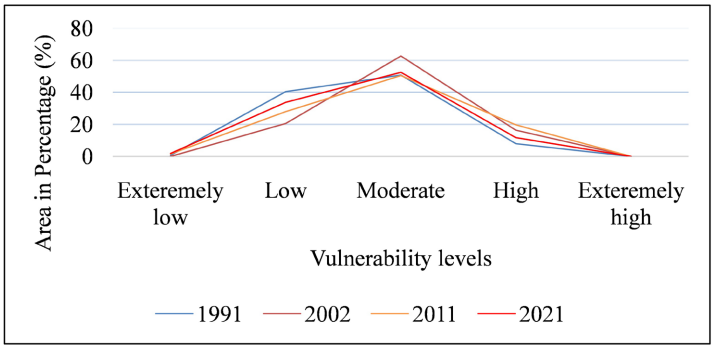

Figure 3. Variation of the percentage areas of the Limuru - Mai Mahiu - Narok hinterlands prone to the detrimental effects of flooding and land subsidence.

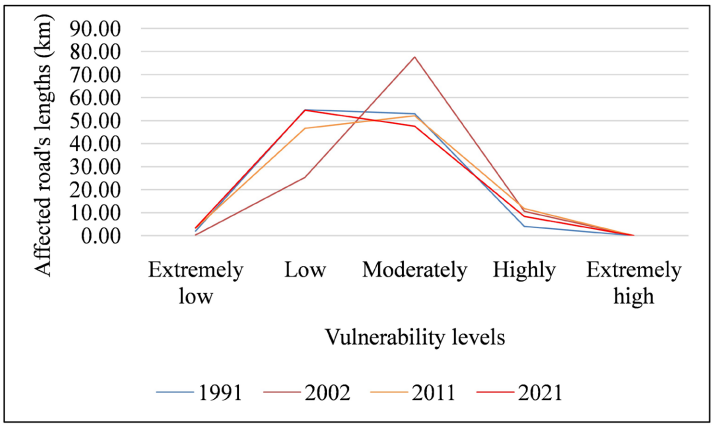

Figure 4. Variations of lengths (km) of the Limuru - Mai Mahiu - Narok road prone to the aggregated effects of flooding and land subsidence.

Moreover, the statistics depicting the vulnerability of Limuru - Mai Mahiu - Narok road to the combined effects of flooding and land subsidence are presented in Figure 4. Statistics exhibit lengths of about 0.28 - 3.41 km, 25.33 - 54.70 km, 47.54 - 77.60 km and 4.05 - 11.80 km of the Limuru - Mai Mahiu - Narok road were vulnerable to extremely low, low, moderate and high geo-environmental vulnerability levels. The statistics also exhibited that only a small fraction of the Limuru - Mai Mahiu - Narok road exhibited the extremely high geo-environmental

vulnerability level. Additionally, the largest portion of the road experienced moderate geo-environmental vulnerability level. The assessment manifested the road was greatly subjected to the detrimental effects of flooding and land subsidence in the year 2002, followed by year 2011, then 2021 and lastly 1991.

2.4.2. Future Vulnerability Scenario of Limuru - Mai Mahiu - Narok Road to the Combined Effects of Flooding and Land Subsidence

The predicted results for vulnerability of Limuru - Mai Mahiu - Narok road to aggregated effects of flooding and land subsidence are presented in Figure 5. The validation results for 2021 produced Kappa coefficient values, that is Kno, Klocation, KlocationStrata, Kstandard, and average index of 0.74, 0.75, 1.0, 0.65, and 0.78, respectively, which ascertained good performance and reliability of the prediction model. The predicted results for 2030 manifested that 1.74%, 24.28%, 48.99%, 24.96%, and 0.03% of hinterlands would register extremely low, low, moderate, high, and extremely high vulnerability levels, respectively (Figure 6). The results depicted that, there would be an exponential increase of area of hinterlands vulnerable to high and extremely high vulnerability levels (Figure 6). Additionally, the results depict regions near Kijabe, Mai Mahiu, Ntulele, Narok, Noolpopong, Ewaso Kendong and the large chunk of southern and south-western parts of hinterlands would be highly affected (Figure 5(c)).

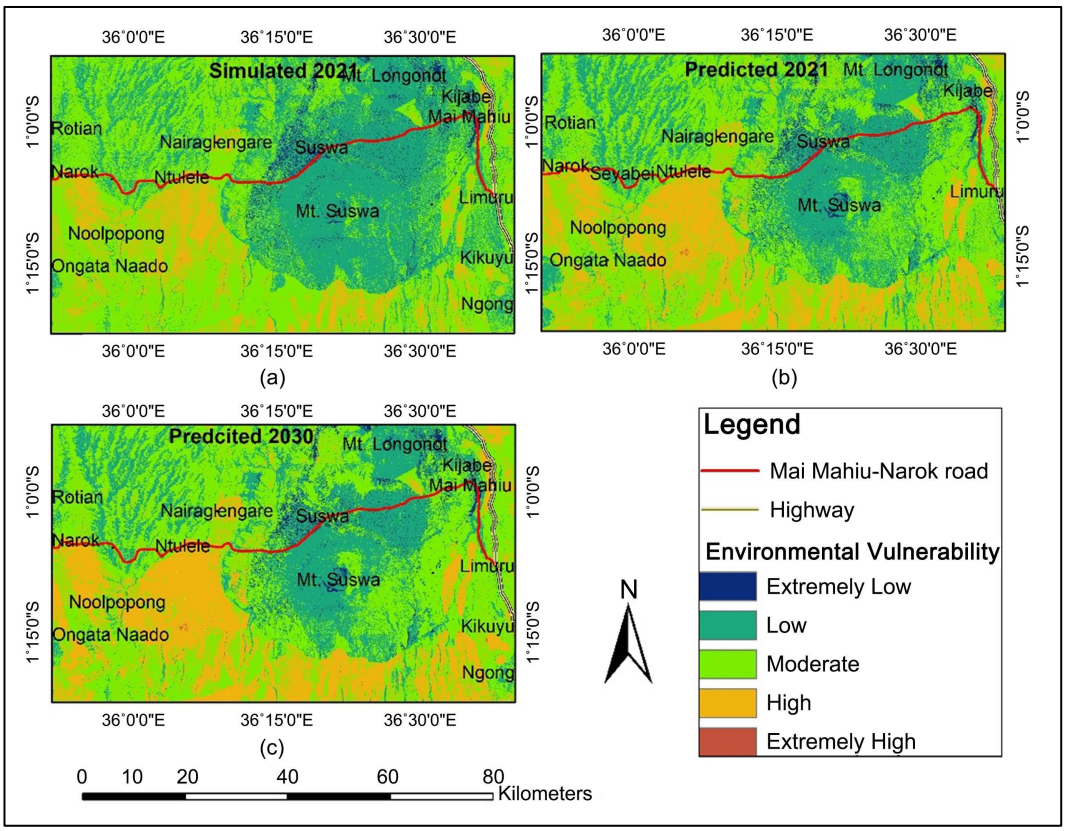

Figure 5. (a) Aggregated hybrid-based simulated d floods and land subsidence vulnerability map for the year 2021, (b) predicted aggregated floods and land subsidence vulnerability map for the year 2021, (c) Predicted aggregated geo-environmental floods and land subsidence vulnerability map for the year 2030.

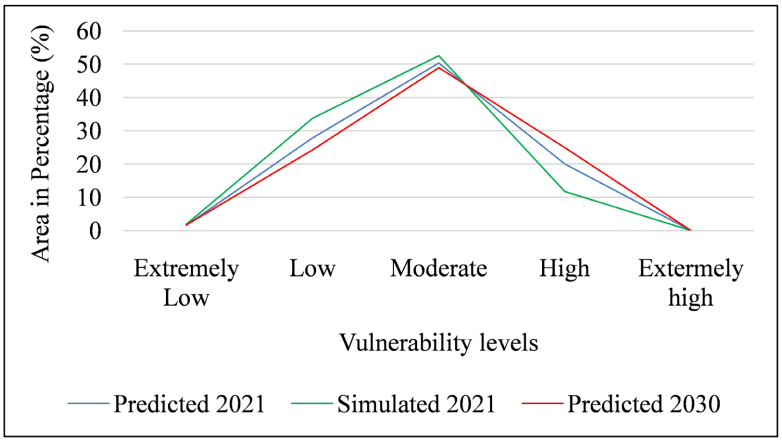

Figure 6. Percentage areas of the hinterlands prone to each category of the combined geo-environmental hazards of floods and land subsidence vulnerability levels.

Moreover, the assessment of Limuru - Mai Mahiu - Narok road exhibited that lengths of about 3.28 km, 39.22 km, 55.01 km, 16.28 km, and 0.00 km would be vulnerable to extremely low, low, moderate, high, and extremely high vulnerable levels, respectively (**Figure 6**). This implies that by 2030, the length of the Limuru - Mai Mahiu - Narok road which would be vulnerable to moderate, high and extremely high levels of vulnerability would increase substantially by about 13.52% compared to the year 2021. Besides, the length of the road which would be vulnerable to extremely low and low levels would shrink by about 13.54% compared to the year 2021 (**Figure 7**). Therefore, the assessment depicts that by the year 2030, the Limuru - Mai Mahiu - Narok road would witness advanced effects of flooding and land subsidence.

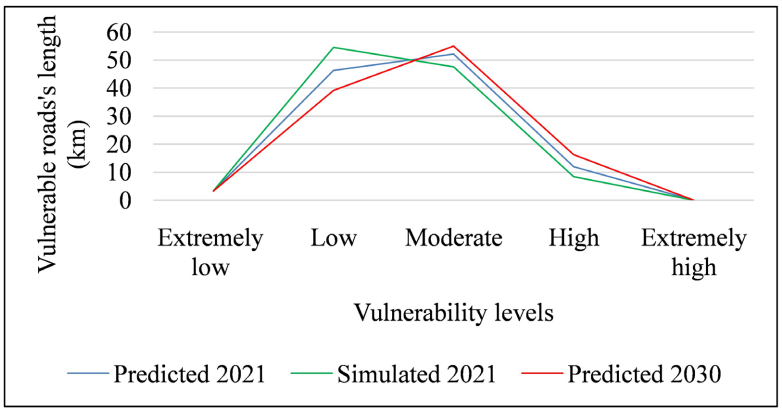

Figure 7. The lengths of the road infrastructure predicted to be affected by aggregated effects of flooding and land subsidence.

2.5. Discussion

2.5.1. Aggregated Effects of Flooding and Land Subsidence on Road Infrastructure

The combined effects of flooding and land subsidence on Limuru - Mai Mahiu - Narok road have manifested that the road is severely stressed by flooding and land

subsidence (Figures 2-4). The results have exhibited that the Limuru - Mai Mahiu - Narok road is susceptible to land subsidence and flooding occasioned by climatic variability, relatively flat route corridor influenced by the physical and environmental processes from the surrounding environs which comprises hills, mountains, escarpments, ravine, and plains [31]. There have been sporadic and untimely cases of flooding and land subsidence on the Limuru - Mai Mahiu - Narok road which snarl-up traffic flow, and reduce the operation activities along this road. The situation could be further aggravated by the fact that the largest section of the Limuru - Mai Mahiu - Narok road lie on a plain dominated by clayey soil, fissures, active geothermal and volcanic activities, tectonic plates movements which exacerbate flooding and land subsidence (Figure 8). This results in road failures as witnessed during heavy rainfall season [31].

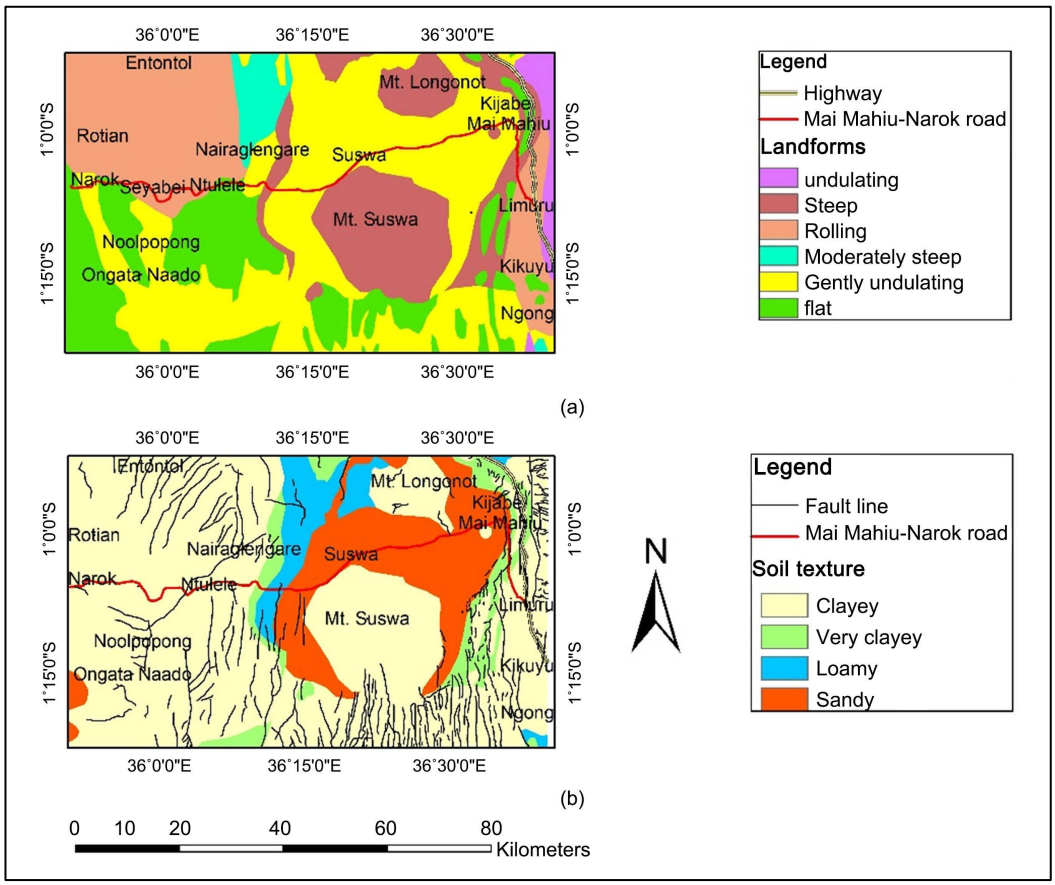

Figure 8. (a) Landforms in the hinterlands where Limuru - Mai Mahiu - Narok Road traverse, (b) Distribution of soil texture and fault lines in the hinterlands of Limuru - Mai Mahiu - Narok Road.

Therefore, the research deduced that the untimely and uncontrolled occurrence of flooding and land subsidence has detrimental effects on Limuru - Mai Mahiu - Narok road which lowers its functionality and resilience especially during rainy seasons [31] [49]. Our research findings have been supported by several and untimely incidences of road closures caused by flooding (Figure 9) and land subsidence (Figure 10) experienced during the rainy season [31].

(a)

(b)

(c)

Figure 9. (a) Snarled- up traffic in the Limuru - Mai Mahiu - Narok road between Duka Moja and Ntulele towns by flooding, (b) Effects of flooding on built-up structure and soil in the hinterlands between Mai Mahiu and Suswa, (c) Flooded region near Ntulele town.

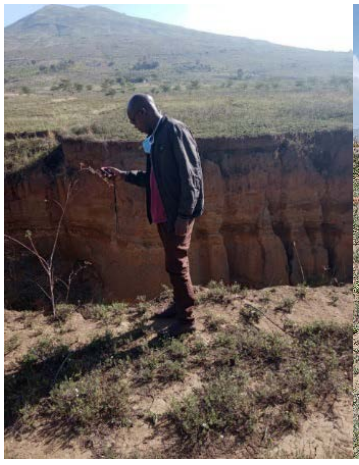

(a)

(b)

(c) (d)

(e)

(f)

(g)

Figure 10. (a) Fissure in the hinterland between Mai Mahiu to Naivasha towns (b) Fissures observed in the hinterland between Mai Mahiu to Suswa towns (c) Fault lines detected in the Ewaso Kendong (d) Faultline noticed in the hinterland near Suswa town (e) Collapsed bridge Near Ntulele town as a result of land subsidence (f) and (g) Fissures cutting the Limuru - Mai Mahiu - Narok Road near Duka Moja shopping center.

2.5.2. Predicted Effects of Flooding and Land Subsidence on the Road Infrastructure

The prediction results depicted that by 2030 the large chunk of Limuru - Mai Mahiu - Narok road would be vulnerable to moderate, high and extremely high vulnerability levels of aggregated effects of flooding and land subsidence (**Figure 5**). The results projected that by 2030, the detrimental effects of flooding and land subsidence would escalate by about 13.52% compared to 2021 (**Figure 6**), which implies more stress will be imposed on the Limuru - Mai Mahiu - Narok road thus aggravating its functionality, serviceability and its durability [20]. Therefore, based on the prediction results, it would be paramount to consider some pro-active measures both engineering and non-engineering to counteract further escalation of the Limuru - Mai Mahiu - Narok road to the detrimental effects of flooding and land [50].

3. Conclusions

The assessment of vulnerability of Limuru - Mai Mahiu - Narok road to flooding demonstrated that the largest chunk of its hinterlands is prone to moderate, high, and extremely high vulnerability levels. It was also noticed that the floods vulnerability levels were sporadic and depended on the prevailing climatic, biophysical and anthropogenic activities but more pronounced during rainy seasons. It exhibited regions such as Narok, Ntulele and some pockets near Mai Mahiu were highly susceptible to flooding during rainfall seasons. Besides, the assessment of vulnerability of hinterlands to land subsidence de depicted that the largest section fell under moderate, high, and extremely high vulnerability levels. The results manifested that more than half of the hinterlands were prone to land subsidence but more pronounced to the south and east of Mt. Suswa and east of Kijabe town. Moreover, some incidences of land subsidence were revealed near Mai Mahiu, Ntulele and Ongata Naado regions. The assessment of combined effects of flooding and land subsidence revealed that the Limuru - Mai Mahiu - Narok road was prone to moderate, high and extremely high vulnerability levels. The vulnerability was dire in the year 2002 where about 77.4% of the road's length registered moderate, high and extremely high vulnerability levels. Besides, the year 2021, was least affected since only about 49.1% of the road's length was vulnerable to moderate, high, and extremely high vulnerability levels. Moreover, the prediction results exhibited that by the year 2030, the length of Limuru - Mai Mahiu - Narok road that would be vulnerable to moderate, high, and extremely high vulnerability level would increase by about 13.52%.

The research deduced that the Limuru - Mai Mahiu - Narok road is vulnerable to the effects of flooding and land subsidence which vary sporadically depending on the prevailing climatic, biophysical, and anthropogenic activities, which escalate during rainy seasons. This calls for identification and implementation of appropriate engineering and non-engineering interventions in order to alleviate further deterioration of this road, thus promoting its resilience for sustainable socio-economic development.

Conflicts of Interest

The authors declare no conflicts of interest.

References

[1] Sun, L., Ma, C. and Li, Y. (2019) Multiple Geo-Environmental Hazards Susceptibility Assessment: A Case Study in Luoning County, Henan Province, China. *Geomatics, Natural Hazards and Risk*, **10**, 2009-2029. https://doi.org/10.1080/19475705.2019.1658648

[2] Kumar, A., Shekhar, S., Tirkey, A.S. and Krishna, A.P. (2020) Geo-Environmental Hazard Vulnerability and Risk Assessment over South Karanpura Coalfield Region of India. In: Kanga, S., *et al.*, Eds., *Sustainable Development Practices Using Geoinformatics*, Wiley, 23-45.

[3] Youssef, A.M. and Abdel Moneim, A.A. (2006) Evaluation of the Geo-Environmental Hazard in Relation to the Future Development Using Geographic Information Systems, East Sohag Area, Egypt. *The 3rd International Conference of Environment and Development in the Arab World*, Vol. 1, 673-692.

[4] Swain, K.C., Singha, C. and Nayak, L. (2020) Flood Susceptibility Mapping through the GIS-AHP Technique Using the Cloud. *ISPRS International Journal of Geo-Information*, **9**, Article No. 720. https://doi.org/10.3390/ijgi9120720

[5] Youssef, A.M., Al-Harbi, H.M., Gutiérrez, F., Zabramwi, Y.A., Bulkhi, A.B., Zahrani, S.A., *et al.* (2015) Natural and Human-Induced Sinkhole Hazards in Saudi Arabia: Distribution, Investigation, Causes and Impacts. *Hydrogeology Journal*, **24**, 625-644. https://doi.org/10.1007/s10040-015-1336-0

[6] Phillips, B.B., Bullock, J.M., Osborne, J.L. and Gaston, K.J. (2021) Spatial Extent of Road Pollution: A National Analysis. *Science of the Total Environment*, **773**, Article ID: 145589. https://doi.org/10.1016/j.scitotenv.2021.145589

[7] Haghizadeh, A., Siahkamari, S., Haghiabi, A.H. and Rahmati, O. (2017) Forecasting Flood-Prone Areas Using Shannon's Entropy Model. *Journal of Earth System Science*, **126**, Article No. 39. https://doi.org/10.1007/s12040-017-0819-x

[8] Wubalem, A., Tesfaw, G., Dawit, Z., Getahun, B., Mekuria, T. and Jothimani, M. (2020) Comparison of Statistical and Analytical Hierarchy Process Methods on Flood Susceptibility Mapping: In a Case Study of Tana Sub-Basin in Northwestern Ethiopia. *Natural Hazards and Earth System Sciences*, **13**, 1-43. https://doi.org/10.5194/nhess-2020-332

[9] Bagheri-Gavkosh, M., Hosseini, S.M., Ataie-Ashtiani, B., Sohani, Y., Ebrahimian, H., Morovat, F., *et al.* (2021) Land Subsidence: A Global Challenge. *Science of the Total Environment*, **778**, Article ID: 146193. https://doi.org/10.1016/j.scitotenv.2021.146193

[10] Ma, T., Du, Y., Ma, R., Xiao, C. and Liu, Y. (2018) Review: Water-Rock Interactions and Related Eco-Environmental Effects in Typical Land Subsidence Zones of China. *Hydrogeology Journal*, **26**, 1339-1349. https://doi.org/10.1007/s10040-017-1708-8

[11] Avilés, J. and Pérez-Rocha, L.E. (2010) Regional Subsidence of Mexico City and Its Effects on Seismic Response. *Soil Dynamics and Earthquake Engineering*, **30**, 981-989. https://doi.org/10.1016/j.soildyn.2010.04.009

[12] Bošnjaković, M., Stojkov, M. and Jurjević, M. (2019) Environmental Impact of Geothermal Power Plants. *Tehnički Vjesnik*, **26**, 1515-1522. https://doi.org/10.17559/TV-20180829122640

[13] Arabameri, A., Chandra Pal, S., Rezaie, F., Chakrabortty, R., Chowdhuri, I., Blaschke, T., *et al.* (2021) Comparison of Multi-Criteria and Artificial Intelligence Models for Land-Subsidence Susceptibility Zonation. *Journal of Environmental Management*, **284**, Article ID: 112067. https://doi.org/10.1016/j.jenvman.2021.112067

[14] Nzau, M. (2013) Mainstreaming Climate Change Resilience into Development Planning in Kenya. IIED Country Report. IIED. http://pubs.iied.org/10044IIED

[15] Kamau, J.W. and Mwaura, F. (2013) Climate Change Adaptation and EIA Studies in Kenya. *International Journal of Climate Change Strategies and Management*, **5**, 152-165. https://doi.org/10.1108/17568691311327569

[16] Le Roux, A., Engelbrecht, F., Paige-Green, P., Verhaeghe, B., Khuluse-Makhanya, S., McKelly, D., *et al.* (2016) Climate Adaptation: Risk Management and Resilience Optimisation for Vulnerable Road Access in Africa: Climate Threats Report. AfCAP Project GEN2014C.

[17] Sultana, M., Chai, G., Chowdhury, S. and Martin, T. (2016) Rapid Deterioration of Pavements Due to Flooding Events in Australia. *Proceedings of* 4*th Geo-China International Conference* (*Geo-China*), 25-27 July 2016, 104-112. https://doi.org/10.1061/9780784480052.013

[18] Abidin, H.Z., Andreas, H., Gumilar, I., Sidiq, T.P. and Gamal, M. (2015) Environmental Impacts of Land Subsidence in Urban Areas of Indonesia. In: *FIG Working Week*, TS 3-Positioning and Measurement, 1-12.

[19] Yu, B., Liu, G., Zhang, R., Jia, H., Li, T., Wang, X., *et al.* (2013) Monitoring Subsidence Rates along Road Network by Persistent Scatterer SAR Interferometry with High-Resolution TerraSAR-X Imagery. *Journal of Modern Transportation*, **21**, 236-246. https://doi.org/10.1007/s40534-013-0030-y

[20] Wilson, S.K. and Wasike, W.S. (2001) Road Infrastructure Policies in Kenya: Historical Trends and Current Challenges. Kenya Institute for Policy Research and Analysis (KIPPRA). http://www.kippra.org/

[21] Sarkar, D. and Mondal, P. (2019) Flood Vulnerability Mapping Using Frequency Ratio (FR) Model: A Case Study on Kulik River Basin, Indo-Bangladesh Barind Region. *Applied Water Science*, **10**, Article No. 17. https://doi.org/10.1007/s13201-019-1102-x

[22] Kalantar, B., Pradhan, B., Naghibi, S.A., Motevalli, A. and Mansor, S. (2017) Assessment of the Effects of Training Data Selection on the Landslide Susceptibility Mapping: A Comparison between Support Vector Machine (SVM), Logistic Regression (LR) and Artificial Neural Networks (ANN). *Geomatics, Natural Hazards and Risk*, **9**, 49-69. https://doi.org/10.1080/19475705.2017.1407368

[23] Ruth, O., Lagat, D. and Lilian, O. (2021) Linking Adaptation and Mitigation toward a Resilient and Robust Infrastructure Sector in Kenya. In: Filho, W.L., *et al.*, Eds., *African Handbook of Climate Change Adaptation*, Springer International Publishing, 2693-2711. https://doi.org/10.1007/978-3-030-45106-6_141

[24] Arnold, K., Le Roux, A. and Khuluse-Makhanya, S. (2018) Implementing a GIS Based Methodology for Determining Highly Vulnerable Rural Access Roads to a Changing Climate in Ethiopia. *Proceedings of Africa GEO* 2018, Pretoria, 17-19 September 2018, 120-138.

[25] Pregnolato, M., Ford, A., Wilkinson, S.M. and Dawson, R.J. (2017) The Impact of Flooding on Road Transport: A Depth-Disruption Function. *Transportation Research Part D*: *Transport and Environment*, **55**, 67-81. https://doi.org/10.1016/j.trd.2017.06.020

[26] Papilloud, T., Röthlisberger, V., Loreti, S. and Keiler, M. (2020) Flood Exposure Analysis of Road Infrastructure—Comparison of Different Methods at National Level. *International Journal of Disaster Risk Reduction*, **47**, Article ID: 101548. https://doi.org/10.1016/j.ijdrr.2020.101548

[27] Adebayo, W.O. and Jegede, O.A. (2010) The Environmental Impact of Flooding on Transportation Land Use in Benin City, Nigeria. *African Research Review*, **4**, 390-400. https://doi.org/10.4314/afrrev.v4i1.58259

[28] Gharizadeh Beiragh, R., Alizadeh, R., Shafiei Kaleibari, S., Cavallaro, F., Zolfani, S., Bausys, R., *et al.* (2020) An Integrated Multi-Criteria Decision Making Model for Sustainability Performance Assessment for Insurance Companies. *Sustainability*, **12**, Article No. 789. https://doi.org/10.3390/su12030789

[29] Gacu, J.G., Monjardin, C.E.F., Senoro, D.B. and Tan, F.J. (2022) Flood Risk Assessment Using GIS-Based Analytical Hierarchy Process in the Municipality of Odiongan, Romblon, Philippines. *Applied Sciences*, **12**, Article No. 9456. https://doi.org/10.3390/app12199456

[30] Kulimushi, L.C., Bashagaluke, J.B., Choudhari, P., Masroor, M. and Sajjad, H. (2021) Novel Combination of Analytical Hierarchy Process and Weighted Sum Analysis for Watersheds Prioritization. a Study of Ulindi Catchment, Congo River Basin. *Geocarto International*, **37**, 8456-8494. https://doi.org/10.1080/10106049.2021.2002426

[31] KeNHA (2020) Geological Study, Feasibility Study, Environmental and Social Impact Study, Preliminary and Detailed Engineer in Design of Suswa—Mai Mahiu (B7) Road Section Tender No: KeNHA/1969/2018. Environmental and Social Impact Assessment Study Report.

[32] Anon (1990) Geological, Volcanological and Hydrogeological Control in the Occurrence of Geothermal Activity in the Area Surrounding Lake Naivasha, Kenya. Republic of Kenya Ministry of Energy and British Geological Survey.

[33] Clarke, M.C.G., Woodhall, D.G., Allen, D. and Darling, G. (1990) Geological, Volcanological and Hydrogeological Controls on the Occurrence of Geothermal Activity in the Area Surrounding Lake Naivasha, Kenya. Ministry of Energy, Kenya and British Geological Survey, Monograph, 138 p.

[34] Satheeshkumar, S., Venkateswaran, S. and Kannan, R. (2017) Rainfall-Runoff Estimation Using SCS-CN and GIS Approach in the Pappireddipatti Watershed of the Vaniyar Sub Basin, South India. *Modeling Earth Systems and Environment*, **3**, Article No. 24. https://doi.org/10.1007/s40808-017-0301-4

[35] Zhan, X. and Huang, M. (2004) ArcCN-Runoff: An ArcGIS Tool for Generating Curve Number and Runoff Maps. *Environmental Modelling & Software*, **19**, 875-879. https://doi.org/10.1016/j.envsoft.2004.03.001

[36] Nayak, T., Verma, M. and Bindu, S.H. (2012) SCS Curve Number Method in Narmada Basin. *International Journal of Geomatics and Geosciences*, **3**, 219-228.

[37] Huang, M., Gallichand, J., Wang, Z. and Goulet, M. (2005) A Modification to the Soil Conservation Service Curve Number Method for Steep Slopes in the Loess Plateau of China. *Hydrological Processes*, **20**, 579-589. https://doi.org/10.1002/hyp.5925

[38] Woodward, D.E., Hawkins, R.H., Jiang, R., Hjelmfelt, A.T., Van Mullem, J.A. and Quan, Q.D. (2003) Runoff Curve Number Method: Examination of the Initial Abstraction Ratio. *World Water & Environmental Resources Congress* 2003, Philadelphia, 23-26 June 2003, 1-10. https://doi.org/10.1061/40685(2003)308

[39] Ibrahim, U. and Mutua, F. (2014) Lineament Extraction Using Landsat 8 (OLI) in Gedo, Somalia. *International Journal of Science and Research*, **3**, 291-296.

[40] Sadiq, S., Muhammad, U. and Fuchs, M. (2021) Investigation of Landslides with Natural Lineaments Derived from Integrated Manual and Automatic Techniques Applied on Geospatial Data. *Natural Hazards*, **110**, 2141-2162. https://doi.org/10.1007/s11069-021-05028-6

[41] Nugroho, U.C. and Tjahjaningsih, A. (2017) Lineament Density Information Extraction Using DEM SRTM Data to Predict the Mineral Potential Zones. *International Journal of Remote Sensing and Earth Sciences*, **13**, 67-74. https://doi.org/10.30536/j.ijreses.2016.v13.a2704

[42] Saaty, T.L. (2003) Decision-Making with the AHP: Why Is the Principal Eigenvector Necessary. *European Journal of Operational Research*, **145**, 85-91. https://doi.org/10.1016/s0377-2217(02)00227-8

[43] Hoque, M.A., Tasfia, S., Ahmed, N. and Pradhan, B. (2019) Assessing Spatial Flood Vulnerability at Kalapara Upazila in Bangladesh Using an Analytic Hierarchy Process. *Sensors*, **19**, Article No. 1302. https://doi.org/10.3390/s19061302

[44] Jafari, S. and Zaredar, N. (2010) Land Suitability Analysis Using Multi Attribute Decision Making Approach. *International Journal of Environmental Science and Development*, **1**, 441-445. https://doi.org/10.7763/ijesd.2010.v1.85

[45] Malczewski, J. (1999) GIS and Multicriteria Decision Analysis. *Geographical Analysis*, **34**, 91-92.

[46] Keyantash, J.A. and Dracup, J.A. (2004) An Aggregate Drought Index: Assessing Drought Severity Based on Fluctuations in the Hydrologic Cycle and Surface Water Storage. *Water Resources Research*, **40**, W09304. https://doi.org/10.1029/2003wr002610

[47] Mokarram, M. and Pham, T.M. (2022) CA-Markov Model Application to Predict Crop Yield Using Remote Sensing Indices. *Ecological Indicators*, **139**, Article ID: 108952. https://doi.org/10.1016/j.ecolind.2022.108952

[48] Wanjala, J.A., Sichangi, A.W., Mundia, C.N. and Makokha, G.O. (2020) Modelling the Dry Season Inundation Pattern of Yala Swamp in Kenya. *Modeling Earth Systems and Environment*, **6**, 2091-2101. https://doi.org/10.1007/s40808-020-00816-8

[49] Gichaga, F.J. (2017) The Impact of Road Improvements on Road Safety and Related Characteristics. *IATSS Research*, **40**, 72-75. https://doi.org/10.1016/j.iatssr.2016.05.002

[50] Onkangi, R.N., Njiiri, M.P., Maklago, E. and Lilian, O. (2019) Vulnerability and Adaptation Levels of the Construction Industry in Kenya to Climate Change. In: Leal, F.W., Ed., *Handbook of Climate Change Resilience*, Springer, 2383-2400.